Journal of Medical Systems (2018) 42: 38
https://doi.org/10.1007/s10916-018-0899-4

EDUCATION & TRAINING

Advances in the Study of the Middle Cranial Fossa through Cutting Edge Neuroimaging Techniques

Juan A. Juanes Méndez [1,2] · Pablo Ruisoto [1,3] · Juan C. Paniagua [4] · Alberto Prats [1,5]

Received: 30 November 2017 / Accepted: 10 January 2018 / Published online: 16 January 2018

Abstract
The objective of this paper is to present a morphometric study of the middle cranial fossa from the study of 87 patients using cutting edge multislice computed tomography scans (32 detectors) and Magnetic Resonance Imaging. The study presents a detailed anatomical-radiological and morphometric analysis of the middle cranial fossa as well as its neurovascular elements in normal conditions. The implications of this investigation in training and clinical contexts are discussed.

Keywords Neuroimaging · Neuroanatomy · Middle cranial fossa · Multislice computed tomography · Magnetic resonance imaging

Introduction

In diagnostic imaging the knowledge of normal anatomy is of great importance, since this depends on an adequate comprehension of the pathological findings and clinically appropriate decision-making. We must emphasize the importance of normal anatomy knowledge for radiologic interpretation. The middle cranial fossa has a complex anatomy due to the bones that constitute it, which in turn have a series of holes through which important neurovascular structures pass. It is essential to know the radiologic anatomy of this skull base area to correctly evaluate and differentiate normal findings from pathology that can affect different structures that constitute it [1–3].

The objective of this paper is to present a morphologic and morphometric analysis of the middle cerebral fossa through cutting edge neuroimaging techniques; we aim to provide a comprehensive, complete, recent and updated anatomical-radiological study of the different structures forming the fossa, and specially, its multiple holes that can be altered by pathological processes and/or work as dissemination canals for infectious-inflammatory and tumoral processes [3–6].

Material and method

Sample

A retrospective analysis of 87 patients was performed at the Salamanca University Hospital, 40 males and 47 females from emergency, internal medicine, psychiatry, neurology, neurosurgery, otolaryngology and maxillofacial surgery services with a mean age of M = 55 years old and a standard deviation SD = 20,

Instruments and techniques

A multidetector computed tomography, an Aquilion TSX 101ª of 32 detectors was used to produce the images. The magnetic resonance and MR angiography studies were made using a General Electric Signa Horizon device of 1,5 Teslas. The

This article is part of the Topical Collection *on Education & Training*

✉ Juan A. Juanes Méndez
jajm@usal.es

1 Visual Med Research Group, University of Salamanca, Salamanca, Spain

2 Departamento de Anatomía Humana, Facultad de Medicina, Universidad de Salamanca, Avda. Alfonso X El Sabio s/n, 37007 Salamanca, Spain

3 European University of Madrid, Madrid, Spain

4 Neurorradiology Section, University Hospital of Salamanca, Salamanca, Spain

5 Laboratory of Surgical Neuroanatomy (LSNA), Human Anatomy and Embryology Unit, Faculty of Medicine, University of Barcelona, Barcelona, Spain

technique MDCT (Multi-Detector Computarized Tomography) was the employed for the study of the middle cranial fossa bone structures while the MR was used to study softer structures and cranial nerves. Finally, the angiography was employed to study vascular elements. Both the CT angiography and MR angiography measured the vessel diameter and identified adjacent structures.

CT acquisition protocols

Two CT scans were obtained, one in anteroposterior projection and the other in lateral position, with a cut interval of 1,5 mm for the skull base and 5 mm for the brain and helical images with volumetric reconstructions of interest areas. The patient remained in supine decubitus position, head towards the gantry, arms alongside the body, with 1 mm slice thickness, collimation of 1 mm, KV of 140 and 1,0 s rotation time for the detection of anatomical details for study in the range of milimeters.

The vascular study using CT angiography was based on two techniques of manual application: on the one hand, 100 cm^3 of intravenous iodinated contrast was administered, followed by 40 cm^3 of physiological solution through a programmed injection pump of 4 cm^3 per second, with a waiting time of 20 s; on the other hand, by placing a ROI (region of interest) in the aortic arch, with the same dose and flow of intravenous contrast than the prior technique, the cuts were initiated when 180 Hounsfield (UH) units were reached instead of where the ROI (aortic arch) was located.

MR acquisition protocol

The standard MR head protocol consisted of a sagittal sequence T1 potentiated Spin Eco (SE), T2 axial Fast Spin Eco (FSE), and coronal FLAIR (Fluid Attenuated Inversion Recovery) FSE T2 potentiated, which is a T2 sequence with suppression of the fluid signal, diffusion study with B1000/DWI and ADC (Apparent Diffusion Coefficient) map.

In the cases of bleeding history a T2 gradient echo was used; in cases of epilepsy the standard head protocol was used plus a coronal FSE T2 projection perpendicular to the temporal lobe; and for the study of the hypophysis the standard protocol was used plus an intravenous inyection.

Advanced image processing and morphometric analysis

The image analysis through volumetric reconstructions was done in a Vitrea^R (Toshiba Medical Systems) work station, and Amira™ computer development tools were used according to the interest of the structure to be studied, MIP (Maximum Intensity Projection) for bone reconstruction and MPR (Multiplanar Reformat) CT angiography for neurovascular soft structures.

Results

The final morphometric analysis of the main foramens and neurovascular elements of the middle cranial fossa are listed in Table 1.

Middle cranial fossa bone structures

The volumetric generation of the middle cranial fossa allowed the distinction of the fossa lmits, sphenoid's greater wing, and the two petrouses of the temporal bone. Its limits are: in its anterior portion through the posterior border of the sphenoid's lesser wing (laterally) and through the sella turcica tubercle (medial), in its posterior portion is the back of the sella turcica (medial) and the superior border of the petrous (lateral margin); relationships: superior with the temporal lobes, hypophysis, cavernous sinus, Meckel's cave; the anterior border of the pharyngeal mucosal, masticator and parapharyngeal Fossa (Fig. 1).

The middle cranial fossa contains a number of orificies radiologically visible, where different vascular and nervious elements are localized.

The foramen rotundum is located in the base of the sphenoid's greater wing, inferolateral to the sphenoidal fissure. In the CT axial images, it appears as a canal that borders the sphenoidal sinus and connects the middle cranial fossa with the pterygopalatine fossa. It can be seen inferolateral to the sphenoidal fissure in the coronal reconstruction. The middle

Table 1 Morphometric analysis results of the most representative elements of the middle cranial fossa: bone, vascular and neural

Elements	Diameter (mm)
Carotid Duct	M = 7,0; SD = 3,3
Vidian Canal	M = 2,5; SD = 0,8
Superior orbital fissure	M = 22,2; SD = 4,1
Meckel's cave	M = 5,6; SD = 1,2
Foramen rotundum	M = 5,2; SD = 1,8
Foramen ovale	M = 7,3; SD = 2,8
Foramen spinosum	M = 2,2; SD = 0,8
Foramen of Vesalius	M = 1,2; SD = 0,5
Internal carotid (cervical segment)	M = 5,1; SD = 3,4
Internal carotid (petrous segment)	M = 4,6; SD = 3,3
Internal carotid (cavernous segment)	M = 4,9; SD = 3,1
Internal carotid (supraclinoid segment)	M = 3,2; SD = 2,1
III cranial nerve	M = 0,9; SD = 0,4
IV cranial nerve	M = 0,8; SD = 0,2
V cranial nerve (preganglionic segment)	M = 4,2; SD = 1,3
VI cranial nerve	M = 1,0; SD = 0,3
Maxillary nerve	M = 1,1; SD = 0,3
Hypophysis	M = 6,0; SD = 4,4

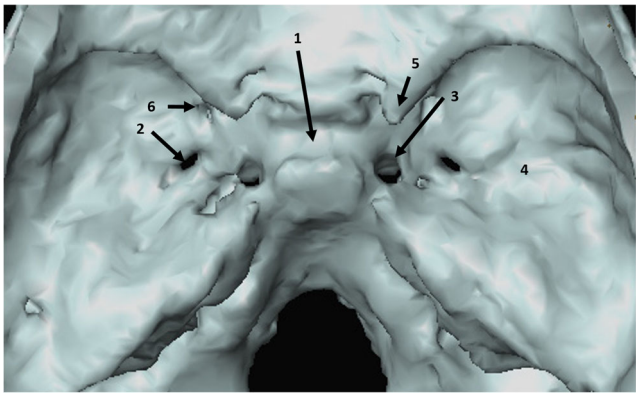

Fig. 1 3D CT reconstruction, using Amira® software, displayed the middle cranial fossa with its different structures. The image shows the sella turcica with its hypofisiary fossa (1), foramen ovale (2), carotid canal (3), greater wing (4), anterior clinoid apophysis (5), and foramen rotundum (6)

wall of the foramen is usually the lateral wall of the sphenoidal sinus, but it can also be found within. The results of the morphometric study suggested, in relation to the foramen rotundum, an average transverse diameter of 5,2 +/ 1,8 mm (Table 1).

The foramen ovale was studied through axial and coronal CT projections. It is shown as it traverses the medial portion of the sphenoid's lesser wing, connecting the middle cranial fossa with the infratemporal fossa and conducting the third branch of the V cranial nerve or mandibular nerve (V3). No variations were found, like the absence of the foramen ovale, changes in its location, confluence with the foramen spinosum, or absence of the medial bone wall, which would involve communication with the foramen lacerum (Fig. 2). The measurement of the foramen ovale's transverse diameter was M = 7,3 mm; SD = 2,8 mm and its anteroposterior diameter was M = 4,6 mm; SD = 1,5 mm.

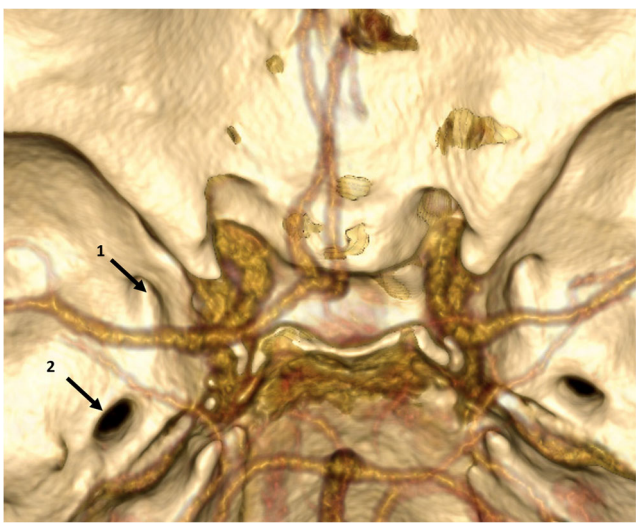

Fig. 2 Endocranial view of the middle cranial fossa in 3D MDCT reconstruction, the foramen rotundum (1) and foramen ovale (2) are seen

The foramen spinosum was studied from CT axial planes in a posteromedial position in the greater wing of the sphenoid and posterolateral to the foramen ovale. Through the foramen ovale runs the middle meningeal artery, the middle meningeal vein and the recurrent branch of the mandibular nerve and, like the foramen ovale, connects the middle cranial fossa with the infratemporal fossa (Figs. 3 and 4). The average transverse diameter was M = 2,2 mm; SD = 0,8 mm (Table 1).

The superior orbital fissure was located in the fore area of the sphenoid, between the greater and lesser wings, and inferolateral to the optic canal. It comprehends the oculomotor nerve (III), trochlear nerve (IV), abducens nerve (VI), ophthalmic nerve (first branch of V) and superior ophthalmic vein (Figs. 3 and 4). The longitudinal and anteroposterior diameter measurement was M = 22,2 mm; SD = 4,1 mm and M = 7,5 mm; SD = 2,7 mm respectively (Table 1).

The vidian canal extends through the sphenoid body and connects the pterygopalatine fossa with the foramen lacerum. It was located in an inferomedial position to the foramen rotundum in CT axial planes; in the inferior region of the sphenoid body, below and interior of the foramen rotundum in coronal planes; and behind the pterygopalatine fossa in sagittal cuts (Fig. 5). The measurement obtained for the craniocaudal diameter was M = 2,5 mm; SD = 0,8 mm (Table 1).

The foramen of Vesalius is found in the greater wing of the sphenoid connecting the middle cranial fossa with the scaphoid fossa, near the origin of the tensor veli palatini muscle, although it can have multiple anatomical variants and confluence with the foramen ovale. It was identified in an anteromedial position to the foramen ovale in CT axial planes, anterolateral to the foramen lacerum and posterolateral to the vidian canal (Fig. 6). The transverse diameter measurement was M = 1,2 mm; SD = 0,5 mm, though it was only identified in 41% of the explorations and the value did not surpass the 2 mm in any of the CT axial sections (Table 1).

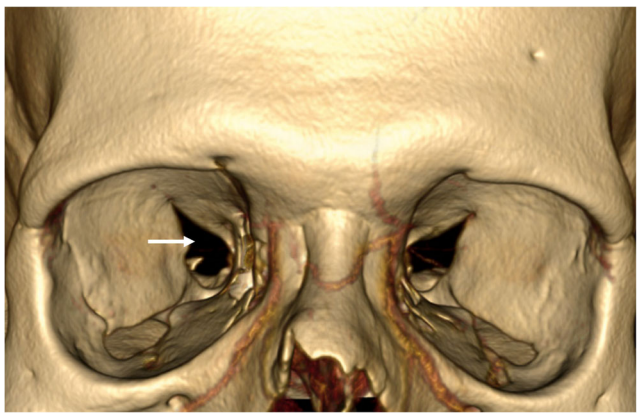

Fig. 3 3D MDCT reconstructions that illustrate the superior orbital fissure (arrow) from a frontal exocranial view and its relationship with the other bone structures

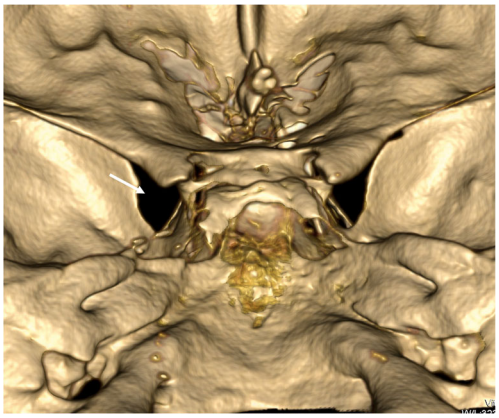

Fig. 4 Multidetector Computed Tomography (MDCT) study with 3D reconstructions and bone protocol, endocranial view, seen from the posterior part, where the superior orbital fissure is observed (arrow)

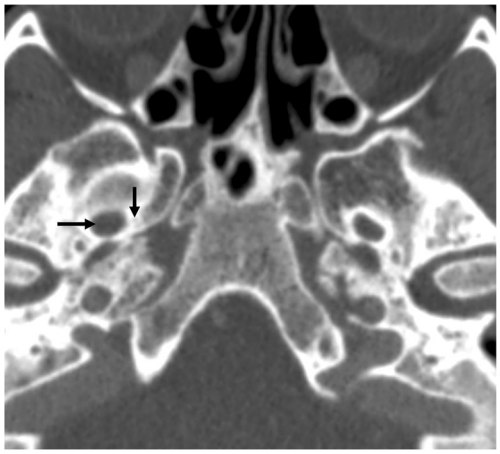

Fig. 6 Axial CT, the foramen of Vesalius (vertical arrow) is seen in the right middle cranial fossa, medial to the foramen ovale (horizontal arrow)

Vascular and neural elements related to the middle cranial fossa

Internal carotid cartery, hypophysis and oculomotor or trigeminal cranial nerves were also analyzed as elements associated with the middle cranial fossa. The internal carotid artery and the carotid sympathetic plexus go through the carotid canal, located between the temporal bone vertex and the sphenoid. It begins in the posteroinferior side of the petrous part of the temporal bone, ascending vertically first and then, after a short journey, bending and continuing in an anterior and medial direction until the vertex of the petrous part. In our study it was seen in 100% of the cases, with a transverse diameter of 7 +/− 3,3 mm (Table 1) in the morphometric analysis.

The internal carotid artery is divided into four segments closely related with the skull base: cervical extracranial, petrous, cavernous and supraclinoid. The ophthalmic artery originates from this last segment. Finally, the internal carotid bifurcates into the medial and anterior artery, which irrigate most of the cerebral hemispheres. The carotid arteries are part of the supra-aortic trunks. The common left carotid emerges directly from the aortic arch, while the common right carotid does so from the brachiocephalic trunk. The external carotid artery has several branches that irrigate extracranial segments. Some of these branches supply the dura mater of the basal and lateral surface. These same meningeal branches also supply the dura mater of the posterior fossa together with the occipital artery. In normal situations, the external carotid is not divided into branches that traverse the skull base, except the medial meningeal artery, a branch of the maxillary artery that intersects the foramen spinosum (Figs. 7, 8, and 9).

The common oculomotor nerve (III), trochlear nerve (IV), oculomotor external nerve (VI) (Fig. 10), ophthalmic nerve (V1) and the superior ophthalmic vein are located in the superior orbital fissure, between the greater and lesser wing of the sphenoid, inferolateral to the optic canal. The maxillary nerve (V2) passes through the foramen rotundum (Fig. 11).

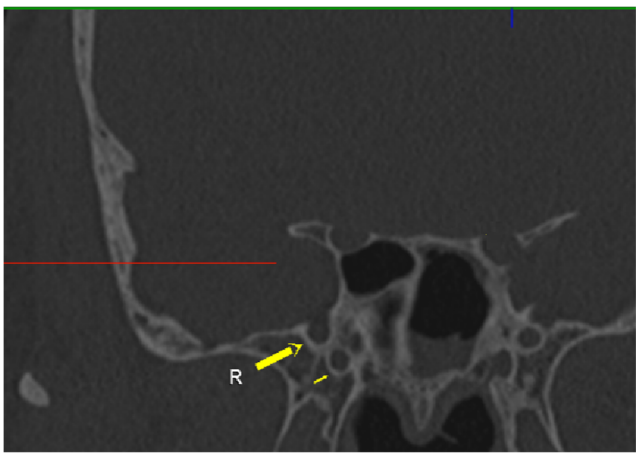

Fig. 5 Coronal CT with the bone window at the foramen rotundum (R) level showing its relationship with the vidian canal (short arrow) in the sphenoid body

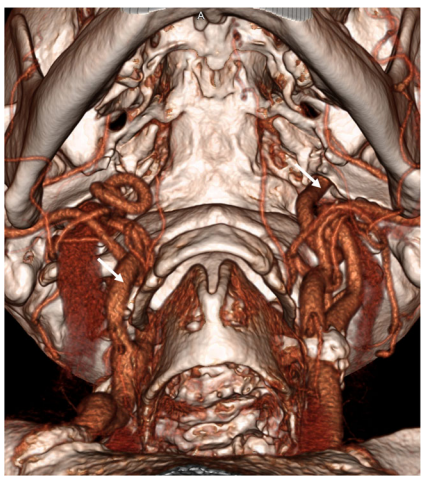

Fig. 7 3D MDCT reconstruction, the carotid canal is seen exocranially with the internal carotid artery traversing it

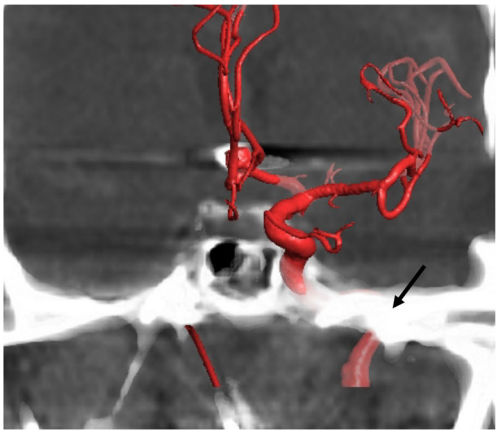

Fig. 8 MDCT carotid artery study with 3D reconstruction in a frontal and inferior plane, exocranial view and its entrance into the skull base is through the carotid canal

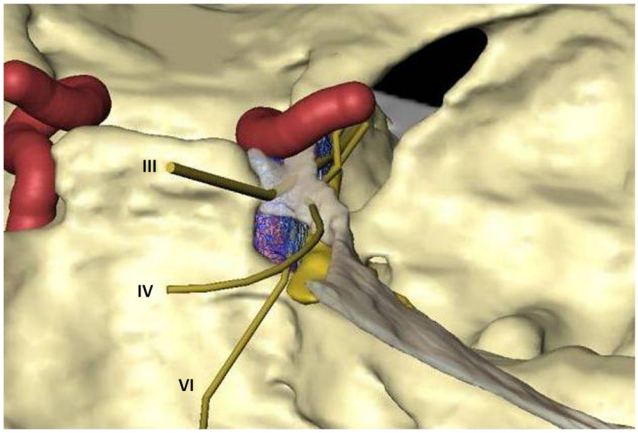

Fig. 10 3D reconstruction using Amira® software, displaying the cavernous sinus (blue), internal carotid arteries (red) and the cranial nerves III, IV and VI, which proceed adjacent to the cavernous sinus to go toward the superior orbital fissure

The superior orbital fissure's morphometric study showed measurements of 22,2 +/− 4,1 × 7,5 +/− 2,7 mm of longitudinal and anteroposterior diameters respectively (Table 1).

Discussion

The great technological developments of recent decades in the field of medicine and specially in diagnostic imaging, has revolutionized the different clinical and surgical specialties by facilitating a better assessment of morphological aspects present in anatomical structures and whose use, currently, is one of the main pillars in decision making for clinical activity.

Diagnostic imaging in the areas of neurology, neurosurgery, maxillofacial surgery and all the specialties dedicated to studying neuroradiology, have experimented these vertiginous developments, even getting to a high percentage of medical and surgical decision making based on radiologic findings.

The study of the skull base, although being a very complex anatomical part of neuroradiology due to the bones that constitute it, which in turn present a series of holes, through which neurovascular structures of great importance pass, and that separate an aseptic cavity (endocranial cavity) from the other extracranial cavities (septic) is adequately done using neuroimaging techniques such as the multidetector computerized tomography, the magnetic resonance and the vascular studies through CT angiography, MR angiography and digital subtraction angiography are the techniques of choice [7–15].

Nowadays we have high value diagnostic tools to study the skull base, most of which are non-invasive and have minimal side effects for the patient's health, except in very special cases where neuroimaging techniques imply an invasive condition.

The research so far on the skull base and specifically on the morphology and morphometry of the middle cranial fossa, are scarce and the ones that exist focus mainly on pathological aspects, making it difficult to do an exhaustive comparison with our study.

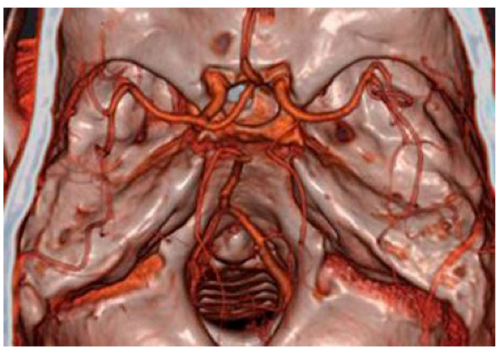

Fig. 9 CT 3D image of the internal carotid artery that illustrates a vascular overlap in the petrous part. Incidentally, an aneurism is observed in the anterior cerebral artery

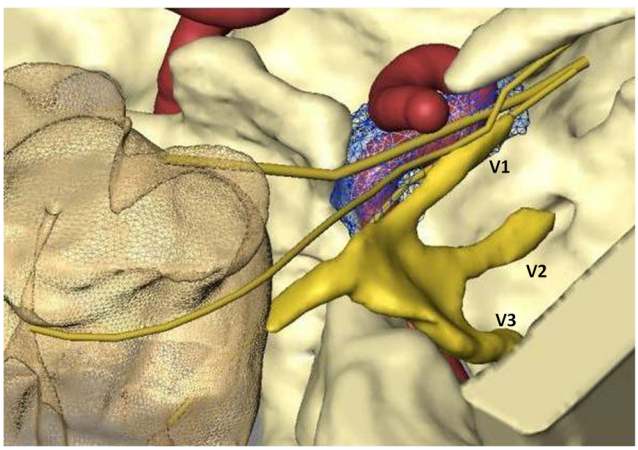

Fig. 11 3D reconstructed image using Amira® software, showing the three branches of the trigeminal nerve (V cranial nerve). V1 (ophthalmic nerve), V2 (superior maxillary nerve) and V3 (mandibular nerve)

The anatomy of the middle cranial fossa is adequately studied through the techniques employed in our research (multidetector computerized tomography, magnetic resonance, CT angiography, MR angiography and digital subtraction angiography).

The bone component of the middle cranial fossa, with its different anatomical details, is studied using computerized tomography, the technique of choice given that besides being fast, non-invasive, inexpensive and highly available, has a high sensibility in the characterization of normal and pathologic bone anatomy. It allows helical acquisitions of 0,6 mm and multiplanar and three-dimensional posterior reconstructions that improve the visualization of its components.

For the analysis of skull base normal anatomy or its anatomical variants, the intravenous contrast is not necessary and is reserved for the study of its pathology in some cases, or for the visualization of the vascular component that goes through it [16–18]. In the analysis of neurovascular components that traverse the middle cranial fossa, we consider that the use of computerized tomography provides non-conclusive data. In the study of cranial nerves, it barely offers indirect data regarding its pathology; nevertheless the use of another diagnostic technique will always be necessary. In the vascular study, without the administration of intravenous contrast, it is not possible to visualize normal brain vessels. Therefore, in our study we used the computerized tomography for the visualization of bone structures, without underestimating its contribution to pathological processes.

The CT angiography and MR angiography are two highly valued techniques in the study of vascular structures that traverse the skull base. The CT angiography is used in most vascular diagnoses in neuroradiology. The key aspects when doing a quality CT angiography are: adequate arterial enhancement during acquisition, complete coverage in the craniocaudal axis of the area that wants to be studied and agreement in the maximum vascular enhancement with acquisition time. Thus, the three components that must be considered are acquisition parameters; dye used and contrast circulation time [7, 19–22].

In summary, the results of this paper offer an anatomoradiological and morphometric study of the middle cranial fossa in the skull base using next generation neuroimaging techniques. Complementarily, the vascular and nervous elements that extend through this structure are analyzed. The radiologic anatomy knowledge of the structures in the skull base is key for the proper study and diagnosis of possible alterations. This study also offers an updated and complete viewpoint with high diagnostic value.

Compliance with ethical standards

Conflict of interest The authors declare that they have no conflict of interest.

Ethical approval All procedures performed in studies involving human participants were in accordance with the ethical standards of the institutional and/or national research committee and with the 1964 Helsinki declaration and its later amendments or comparable ethical standards.

References

1. Borges, A., Imaging of the central skull base. *Neuroimaging Clin. N. Am.* 19:441–468, 2009.
2. Harnsberger, H. R., Osborn, A. G., Ross, J. S., Moore, K. R., Salzman, K. L., Carrasco, C. R., Hamilton, B. E., Davidson, H. C., and Wiggins, R. H., Diagnostic and surgical imagen anatomy. *Brain. Head and Neck. Spine. Amirsys*. 2009.
3. Oishi, M., Fukuda, M., Ishida, G., Saito, A., Hiraishi, T., and Fujji, Y., Prediction of the microsurgical window for skull-base tumors by advanced three-dimensional multi-fusion volumetric imaging. *Neurol. Med. Chir.* 51:201–207, 2011.
4. Ceylan, S., Koc, K., and Anik, I., Extended endoscopic approaches for midline skull- base lesion. *Neurosurg. Rev.* 32:309–319, 2009.
5. Kwak, R., and Shatzkes, D., Transdural spread of glioblastoma through the foramen ovale with presentation as a masticator space mass. *AJNR Am. J. Neuroradiol.* 30:808–810, 2009.
6. Bo, W., Sheng-Tian, W., Zhi, L., and Pi-Nan, L., Anterior and middle skull base reconstruction after tumor resection. *Chin. Med. J.* 123:281–285, 2010.
7. Luyando, L. H., Blanco, J., and Llano, R., Estudio vascular con tomografía computarizada. *Sociedad Española de Radiología Medica* 1:1–8, 2008.
8. Morhard, D., Fink, C. H., Becker, C. H., Reiser, M. F., and Nikolaou, K., Value of automatic bone subtraction in cranial CT angiography: comparison of bone subtracted vs. standard CT angiography in 100 patients. *Eur. Radiol.* 18:974–82, 2008.
9. Sharma, B. S., Gupta, A., Ahmad, F. U., Suri, A., and Mehta, V. S. Surgical management of giant intracranial aneurisms. *Clin. Neurol. Neurosurg.* 110:674–81, 2008.
10. Amemya, S., Aoki, S., and Ohtomo, Cranial nerve assessment in cavernous sinus tumors with contrast-enhanced 3D fast-imaging employing steady-state acquisition MR imaging. *Neuroradiology.* 51:467–470, 2009.
11. Lv, X., Jiang, C. H., Li, Y., Yang, X., and Wu, Z., Endovascular treatment for pediatric intracranial aneurysms. *Neuroradiology* 51: 749–54, 2009.
12. Ma, R., Liu, C., Deng, K., Song, S. J., Wang, D. P., and Huang, L., Cerebral artery evaluation of dual energy CT angiography with dual source CT. *Chin. Med. J.* 123:1139–44, 2010.
13. Yagy, A., Sato, N., Takahoshi, A., Morita, H., Amanuma, M., Endo, K., and Takeuchi, K., Added value of the contrast-enhanced CISS imaging in relation to conventional MR images for the evaluation of intracavernous cranial nerve lesions. *Neuroradiology.* 52:1101–1109, 2010.
14. Linn, J., Peters, F., Moriggl, B., Naidich, T. P., Brückmann, H., and Yoursy, I. The jugular foramen: Imaging strategy and detailed anatomy at 3T. *AJNR* 30:34–41, 2009.
15. Uchino, A., Saito, N., Okada, Y., and Inoue, K., Carotid-anterior cerebral artery anastomosis on MR angiography: a university hospital-based study. *Neuroradiology.* 54:13–18, 2011.
16. Swartz, J. D., and Faerer, E. N., Congenital malformations of the external and middle ear: high-resolution CT findings of surgical import. *AJR Am. J. Roentgenol.* 501–6, 1985.
17. Borges, A., and Casselman, J., Imaging the trigeminal nerve. *Eur. J. Radiol.* 74:323–340, 2010.
18. Reichelt, A., Zeckey, C. H., Hildebrand, F., Grosshennig, A., Shin, H. O., Galanski, M., and Keberle, M., Imaging of the brain in

polytraumatized patients comparing 64-row spiral CT with incremental (sequential) CT. *Eur. J. Radiol.* 81:789–93, 2012.

19. Lell, M., Ruehm, S. G., Kramer, M., Panknin, C., Habibi, R., Klotz, E., and Villablanca, P., Cranial computed tomography angiography with automated bone subtraction: a feasibility study. *Investig. Radiol.* 44:38–43, 2009.
20. Zhang, L. J., Wu, S. Y., Niu, J. B., Zhang, Z. L., Wang, H. Z., Zhao, Y. E., Chai, X., Zhou, C. S., and Lu, G. M., Dual-energy CT. Angiography in the evaluation of intracranial aneurysms: image quality, radiation dose, and comparison with 3D rotational digital subtraction angiography. *AJNR Am J Roentgenol* 194:23–30, 2010.
21. Luo, Z., Wang, D., Sun, X., Zhang, T., Lui, F., and Dong, D., Comparison of the accuracy of subtraction CT angiography performed on 320-detector row volume CT with conventional CT angiography for diagnosis of intracranial aneurysms. *Eur. J. Radiol.* 81:118–122, 2012.
22. Kuroda, Y., Hosoya, T., Oda, A., Ooki, N., Toyoguchi, Y., Murakami, M., Kanoto, M., Sugawara, C., Honma, T., Sugai, Y., and Nemoto, K., Inverse-direction scanning improves the image quality of whole carotid CT angiography with 64-MDCT. *Eur. J. Radiol.* 80:749–754, 2011.